

Mn promotion effects in Co/TiO₂ Fischer–Tropsch catalysts as investigated by XPS and STEM-EELS

Fernando Morales^a, Frank M.F. de Groot^a, Onno L.J. Gijzeman^a, Ad Mens^a, Odile Stephan^b, Bert M. Weckhuysen^{a,*}

^a Department of Inorganic Chemistry and Catalysis, Utrecht University, Debye Institute, Sorbonnelaan 16, 3584 CA Utrecht, The Netherlands

^b Laboratoire de Physique des Solides, Université Paris-Sud, 91405 Orsay cedex, France

Received 15 September 2004; revised 25 November 2004; accepted 26 November 2004

Available online 13 January 2005

Abstract

The addition of small amounts of Mn to a Co/TiO₂ catalyst affects the catalytic performance in the Fischer–Tropsch synthesis (FTS) by increasing the activity and suppressing the CH₄ yield. These variations in the catalyst selectivity are due to Mn promotion effects that influence the final catalyst active site distribution, playing a role under reaction conditions. The use of STEM-EELS and XPS has provided more insight into the location of Mn as a function of the catalyst surface composition observed after the main preparation steps, that is, calcination and reduction. XPS shows that after calcination the catalysts contain mainly a Co₃O₄ phase, and that after 4 h of reduction in H₂ flow at 350 °C, a fair fraction of the Co₃O₄ is fully reduced to Co⁰. The STEM-EELS measurements reveal the existence of a clear Co–Mn association in the calcined catalyst, in which the Mn apparently forms a mixed oxidic phase with the Co particles and thus causes a decrease in the Co reducibility with respect to a Mn-free Co/TiO₂ catalyst. The Mn tends to segregate over the TiO₂ support after reduction, as indicated by the increase in the Mn/Co and Mn/Ti atomic ratios obtained from XPS. Hence, the Mn compounds migrate from the Co particles and are enriched at the surface of the TiO₂ support during Co₃O₄ reduction to Co⁰. However, the STEM-EELS images obtained for the reduced catalyst reveal a remaining Co–Mn interaction, which presumably causes the promotion effect in FTS.

© 2004 Elsevier Inc. All rights reserved.

Keywords: Fischer–Tropsch synthesis; Co-based catalysts; Mn promotion; XPS; STEM-EELS

1. Introduction

The outcome of many catalytic reactions can be influenced by the introduction of small amounts of promoter elements. Some promotion examples are the addition of alkali metals to Fe- and Ru-based ammonia synthesis catalysts [1] and Ag-based epoxidation catalysts [2,3]. A catalyst promoter is defined as an element or compound without catalytic activity by itself, but when it is added to an active catalyst, it enhances the catalyst's activity, selectivity, and/or stability. Two types of promoter elements are normally considered: structural promoters, which increase the

number of exposed metal sites and therefore improve the metal-time yield, and textural promoters, which increase the reaction rate per exposed metal site, that is, the turnover frequency.

In the Fischer–Tropsch synthesis (FTS), a mixture of CO and H₂ (syngas) is transformed into long-chain hydrocarbons with the use of a Co-based catalyst and favorable reaction conditions. This process makes it possible to obtain high-purity transportation fuels from feedstocks other than crude oil, such as natural gas, charcoal, or biomass. These raw materials are first converted into syngas by partial oxidation or steam reforming processes [4]. Co-based catalysts are known to be commercially attractive for FTS because of their high productivity for long-chain paraffins [5] and low deactivation rates. The Co active phase is generally deposited over an oxidic support, for example, SiO₂,

* To whom correspondence should be addressed.

E-mail address: b.m.weckhuysen@chem.uu.nl (B.M. Weckhuysen).

Al₂O₃, or TiO₂, which provides good mechanical strength and thermal stability under reaction conditions [6]. Other potential supports, such as carbon nanofibers, are currently under investigation as well [7]. In recent decades several FT promoter elements (Pt, Re, Ru, and Mn) have been investigated. Pt and Re were reported to enhance the reducibility of the Co sites by means of H₂ spillover and, hence, to enhance the Co dispersion achieved in the active catalyst [8, 9]. Iglesia et al. found that Ru plays a role as a textural promoter for Co-supported catalysts, increasing the activity per active site [10]. Nevertheless, the use of Mn as a promoter in Co-based catalysts is reported only a few times in the literature [11,12]. These papers deal with the potential of Mn to shift the product distribution in FTS by increasing the olefin selectivity and decreasing the undesired CH₄ production. Other works [13,14] report that MnO acts as a CO shift converter promoter and thus catalyzes the water-gas shift reaction (i.e., the transformation from CO + H₂O to H₂ + CO₂). The occurrence of this reaction can influence the reaction kinetics in the FTS and may be interesting when a rich CO syngas composition is used (e.g., the syngas obtained from high-temperature coal gasification [15]). Recently, we reported the importance of using a suitable catalyst preparation procedure to obtain a Mn promotion effect [16]. The exact role of Mn and its influence on the electronic state of the supported Co particles remained unclear, however.

High-energy electron energy-loss spectroscopy (EELS) offers a unique opportunity to correlate spectroscopic information with detailed structural knowledge of a material [17]. In TEM-EELS used as a transmission scattering experiment, a monochromatic beam of electrons is incident on the sample, and the changes in energy of the beam are measured as the beam is propagated through the material. Hence, the EELS spectra provide detailed information about the chemical composition of the material under study. Furthermore, this technique makes possible the construction of detailed elemental chemical maps, which can be processed with a spatial resolution of a fraction of a nanometer.

In a previous study [18] we explored the effect of Mn on TiO₂-supported Co₃O₄ particles by applying soft X-ray absorption spectroscopy to investigate the Co valence as a function of the reduction temperature. It was shown that the addition of Mn reduces the amount of surface Co⁰ after reduction in H₂. The goal of the present work is to understand the role of Mn in Co-based FTS reactions through the use of a combination of X-ray photoelectron spectroscopy (XPS), scanning transmission electron energy loss spectroscopy (STEM-EELS), and catalytic testing. It will be shown that MnO_x particles are largely interacting with supported cobalt oxide particles, leading to a decreased metallic behavior, which results in a higher cobalt-time yield and decreased methane production.

2. Experimental

2.1. Preparation of catalysts

Two TiO₂-supported catalysts were synthesized with the homogeneous deposition precipitation (HDP) technique to load the Co onto the support and the incipient wetness impregnation (IWI) technique to load the Mn. Commercial Degussa P25 titania (surface area 45 m²/g, pore volume 0.27 cm³/g) was used as the support material. The titania powder was suspended in an aqueous solution containing cobalt nitrate (Acros Organics, p.a.), and the pH was slowly increased by urea decomposition at 90 °C under continuous stirring for 18 h. After drying at 110 °C overnight, the material was sieved (0.22–0.50 mm), and a portion was calcined in air at 400 °C for 4 h with a heating rate of 5 °C/min, yielding the Co/TiO₂ catalyst. For the preparation of the Mn-promoted catalyst the other portion of the Co/TiO₂ was impregnated with an aqueous solution of manganese nitrate (Merck, p.a.) followed by the same calcination procedure described above, producing the Co/Mn/TiO₂ catalyst. The Co and Mn loadings of both calcined samples were determined by X-ray fluorescence (XRF) analysis, and the loadings were 7.5 wt% Co and 2 wt% Mn in the promoted catalyst and 7.5 wt% Co in the unpromoted catalyst. A high-purity Co₃O₄ (Merck, p.a.) was used as a reference for the XPS measurements.

2.2. Scanning transmission electron energy loss spectroscopy

Scanning transmission electron energy loss spectroscopy (STEM-EELS) measurements were performed on the fresh calcined catalysts and on the catalysts after a reduction in H₂ flow at 350 °C for 12 h, followed by a passivation in CO₂ flow at 150 °C. To investigate the metal distributions, the oxygen K edge and the titanium, manganese, and cobalt L_{2,3} edges were monitored with a 100-keV STEM instrument (VG HB 501) equipped with a field emission source and a parallel Gatan 666 EELS spectrometer. The instrument was in operation in Orsay and produced EELS spectra with 0.5-eV energy resolution and subnanometer spatial resolution within a typical acquisition time of less than a second per pixel. More specifically, the subnanometer probe (typically 0.5 nm in diameter) could be positioned with an accuracy higher than 0.2 nm on the sample, and it could scan the sample digitally with spatial increments as small as 0.3 nm, as described in more detail by Stephan et al. [17]. The Co/Mn/TiO₂ samples were first sonicated in ethanol and then dropped on a holey amorphous carbon film supported on a copper grid. After the sample was scanned, appropriate areas were selected for measurement of detailed 2D TEM-EELS images. For the calcined samples we analyzed in detail three chemical maps that contain six Co₃O₄ particles, whereas for the reduced/passivated samples we investigated six chemical maps containing 12 Co⁰ particles.

2.3. X-ray photoelectron spectroscopy

XPS data were collected with a Vacuum Generators system, with the use of a CLAM-2 hemispherical analyzer for electron detection. Nonmonochromatic Al (K_{α}) X-ray radiation was used, at an anode current of 20 mA and 10 keV. XPS measurements of both catalysts were performed before and after in situ reduction treatments in H_2 flow at $350^\circ C$ for 2 and 4 h inside an in situ reaction chamber. This chamber was connected to the vacuum system of the spectrometer, allowing the samples to be transferred into the measurement chamber without exposure to air after the H_2 treatments. The binding energies obtained for Co_{2p} , Ti_{2p} , and Mn_{2p} photoelectron peaks were corrected for charge shifts, with the use of the $C\ 1s = 285\ eV$ peak as reference. Co_3O_4 was also measured and corrected for charge shifts, with the $C\ 1s = 285\ eV$ peak as reference. In addition, we used the 2p peaks of the three elements (Co, Ti, and Mn) in the catalysts for quantitative analysis to calculate the atomic ratios of the elements, assuming the composition of the samples to be uniform throughout the area probed by XPS. To calculate the 2p peak areas of the three elements, we subtracted backgrounds according to the procedure suggested by Shirley [19]. These areas are proportional to the number of photoelectrons produced for a given flux of incoming X-rays (ϕ_x), which is the number of incident X-ray photons per $cm^2\ s$. The number of photoelectrons (N) produced per ϕ_x depends only on the material constants:

$$\frac{N}{\phi_x} = \sigma\rho\lambda,$$

where A is the probed area of the sample, σ is the cross section, ρ is the atomic density, and λ is the inelastic mean free path, provided that only electrons moving in a path perpendicular to the surface are detected. For an infinitely thick sample we define I_{obs} as the observed intensity, which can be calculated for any chemical compound if σ (tabulated for all chemical compounds), ρ , and λ are known. Thus, the atomic ratio of the elements A and B can be calculated from

$$\frac{\rho^A}{\rho^B} = \frac{I_{obs}^A}{I_{obs}^B} \frac{ASF^B}{ASF^A},$$

where ASF are the sensitivity factors calculated with the cross section values published elsewhere [20], according to the formula

$$ASF = \sigma\lambda \frac{1}{\sqrt{E_{Kin}}\ (eV)}.$$

2.4. Catalyst testing

FTS tests were carried out in a stainless-steel reactor (volume of about 1 ml) designed to permit the operation of up to 6 reactors, which can be stacked on top of each other. Feed gases are supplied from the top of the reactor over the catalyst and products also leave the reactor at the top. Silco steel treatment of the inside of the reactor is applied to make

it virtually inactive. The reaction temperature is measured with a chromel/alumel thermocouple. Before the reaction was started, the samples were activated in situ in H_2 flow at $300^\circ C$ for 1 h. The reaction was carried out at $220^\circ C$, at a H_2/CO ratio of 2, and at pressures of 1, 4, 8, and 18 bar. The residence time was kept constant by adjustment of the syngas flow going into the reactor to 1, 4, 8, and 18 ml/min. Hence, the CO conversions were kept low ($<1\%$) to create real differential conditions and to prevent condensation of high-weight products. The product composition was analyzed on-line with a Chrompack-9001 gas chromatograph equipped with a Poraplot Q column, for the separation of C_1 to C_5 and a CP-Sil-5 column for the separation of C_6 to C_{20} , and flame ionization detectors (FIDs).

3. Results and discussion

3.1. X-ray photoelectron spectroscopy

Fig. 1 shows the Co 2p XPS spectra for $Co/Mn/TiO_2$ and Co/TiO_2 after calcination and a bulk Co_3O_4 material measured for comparison. The shapes and energy positions of the two photoelectron peaks are nearly the same in the catalysts and in the bulk Co_3O_4 ($2p_{3/2} = 779.9\ eV$ and $2p_{1/2} = 795.2\ eV$). These energy values for Co_3O_4 are in agreement with other work [21], indicating that Co_3O_4 is the main cobalt phase contained in the surface of both catalysts after calcination. This compound has a spinel-type structure, in which oxygen atoms are arranged in fcc and Co^{2+} (T_d) and Co^{3+} (O_h) cations are located in tetrahedral and octahedral coordination, respectively [22]. Detailed interpretations of the Co 2p XPS spectral shapes are presented in papers by Okada and Kotani [23] and van Elp et al. [24]. Only a slight shift in the energy position of the Co 2p peaks ($\sim 0.2\ eV$)

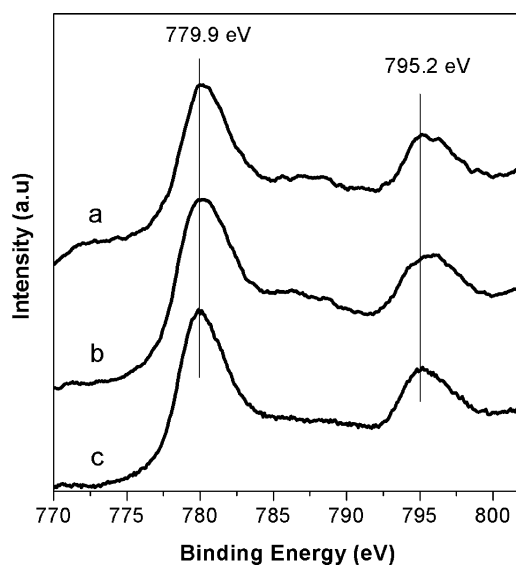


Fig. 1. Co 2p XPS region of Co_3O_4 (a), and Co/TiO_2 (b) and $Co/Mn/TiO_2$ (c) catalysts after calcination.

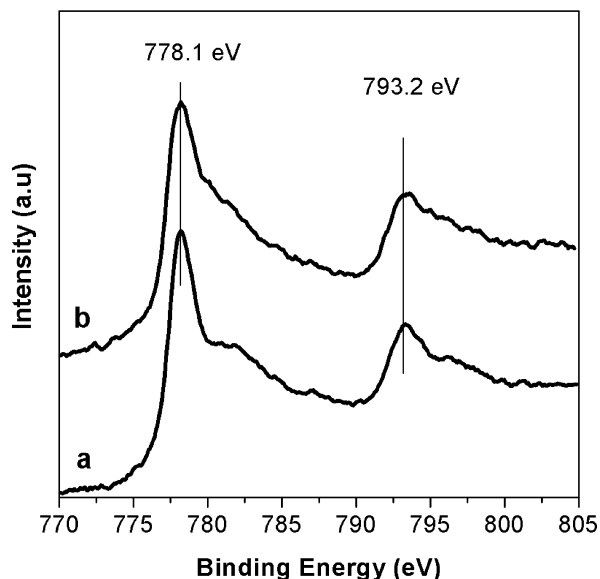


Fig. 2. Co 2p XPS region of Co/TiO₂ (a) and Co/Mn/TiO₂ (b) after 4 h of reduction in a H₂ flow at 350 °C.

is found in a comparison between bulk Co₃O₄ and the catalysts. This might be due to the existence of more Co²⁺ in the catalyst than in bulk Co₃O₄. The existence of very small amounts of highly dispersed CoTiO₃ or CoO species, which are likely to be formed as a result of the temperature treatments [25], is also feasible, though in a minor quantity.

Co 2p spectra for the catalysts obtained after 4 h of reduction are presented in Fig. 2. The binding energies of the photoelectron peaks are now shifted to lower values (Co 2p_{3/2} = 778.1 eV and Co 2p_{1/2} = 793.2 eV), and, moreover, the peaks have narrowed. These binding energies and peak shapes are characteristic of metallic cobalt, indicating a high level of reduction to Co⁰ in the catalysts. However, the presence of a shoulder at higher energies (~6 eV) in both spectra suggests the existence of unreduced CoO in addition to Co⁰. This shoulder is more pronounced in the Co/Mn/TiO₂ catalyst, indicating a lower extent of reduction achieved in this catalyst due to the presence of MnO. This is in line with our recent results obtained by soft X-ray absorption spectroscopy, where a lower amount of Co⁰ was measured after in situ reduction treatments [18].

Mn 2p spectra for Co/Mn/TiO₂ obtained before and after 4 h of reduction are presented in Fig. 3. The energy position of the 2p_{3/2} peak increases after reduction from 641.8 to 642.5 eV. These values indicate that Mn is always present in the oxidic form and cannot be reduced to Mn⁰ at such low temperatures. The binding-energy value found before reduction corresponds to Mn in the trivalent state (Mn^{III}) according to the literature [26]. Nevertheless, the increase in the binding energy obtained after reduction does not explain the change in oxidation state, since it is not possible to determine it from the energy position of either the 2p or 3p peaks [27]. The valence of Mn at the surface of Co/Mn/TiO₂ was previously measured by soft X-ray absorption [18], wherein a

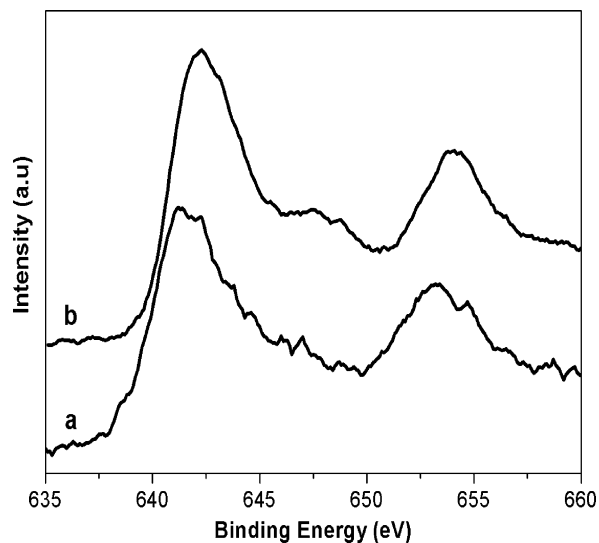


Fig. 3. Mn 2p XPS region of Co/Mn/TiO₂ catalysts after calcination (a) and after 4 h reduction (b).

Table 1

Atomic ratios of Co/TiO₂ and Co/Mn/TiO₂ catalysts after the different treatments as obtained with XPS

	Atomic ratio			
	Co/TiO ₂	Co/Mn/TiO ₂		
		Co/Ti	Mn/Co	Mn/Ti
After calcination ^a	0.32	0.24	0.54	0.13
After reduction ^b 2 h	0.25	0.27	0.86	0.22
After reduction ^b 4 h	0.24	0.28	0.88	0.25

^a In airflow at 400 °C during 4 h.

^b In H₂ flow at 350 °C inside the XPS chamber.

mixture of Mn^{II}, Mn^{III}, and Mn^{IV} was obtained for the calcined catalysts, and Mn^{II} was obtained only after a reduction treatment.

To investigate the changes in the surface composition occurring after reduction, the atomic ratios of all of the elements were compared in both catalysts before and after reduction. The XPS quantitative data are listed in Table 1, which gathers the elemental atomic ratios (Co/Ti, Mn/Co, and Mn/Ti) for both catalysts after calcination and after 2 and 4 h of reduction. After calcination a lower Co/Ti ratio is obtained for the Mn-containing catalyst. This suggests a possible physical association of Co₃O₄ and MnO_x or the coverage of Co₃O₄ by MnO_x upon the second impregnation and calcination. This would lead to a weaker Co signal and therefore to a lower Co/Ti ratio. The Co/Ti ratios change differently in the two catalysts with the reduction treatment. In the Co/TiO₂ catalyst, the Co/Ti ratio decreases from 0.32 to 0.24 after 4 h of reduction. This decrease may be due to the changes in the atomic densities occurring upon the phase transition from Co₃O₄ to Co⁰ and to a decrease in the inelastic mean free path of the electrons in Co⁰ with respect to Co₃O₄ [21]. In the case of the Co/Mn/TiO₂ catalyst the reduction has an opposite effect on the atomic ratios, since a slight increase in Co/Ti from 0.24 to 0.28 is obtained. This

points to a decrease in the Ti intensity and an increase in the Co intensity upon reduction when Mn is contained in the catalyst. Moreover, the Mn/Co and Mn/Ti ratios clearly increase with reduction time (Table 2), as a result of an increase in the Mn signal. These changes in the atomic ratios are likely related to the enrichment of MnO at the surface of the catalyst, which causes an increase in the Mn/Co, Mn/Ti, and Co/Ti ratios after reduction [28]. This fact can be explained by the migration of the MnO particles toward the support as soon as the Co_3O_4 is reduced to Co^0 . After reduction the manganese remains in the oxidic state, mainly as MnO [18,29], and therefore has a higher affinity for the oxidic support than for metallic Co^0 . This migration of MnO from the Co^0 particles leads to an increase in the Co signal since Co^0 is no longer covered or mixed with MnO_x . This accounts for the different trend observed in the Co/Ti ratios after reduction. TiO_2 P25 material contains around 75% anatase phase. On the anatase surface the concentration of coordinatively unsaturated Ti^{4+} ions varies between 4.5 and

$7 \text{ Ti}^{4+}/\text{nm}^2$, and the concentration of the insolated $\text{Ti}^{4+}\text{-OH}$ groups is not more than $0.5 \text{ OH group}/\text{nm}^2$ [30,31]. Considering the anchoring sites as the hydroxyl groups and in the vicinity of the cus Ti^{4+} ions, and assuming one Mn^{n+} ion per two Ti^{4+} ions [32], a monolayer coverage would be reached at around 1.9 wt% Mn. This means that in the Co/Mn/TiO_2 , the loading of 2 wt% Mn is enough to reach more than a monolayer coverage over the TiO_2 surface. This argument accounts for the observed changes in the atomic ratios, since a covering of the TiO_2 surface by MnO would cause a significant decrease in the Ti signal. This effect is indicative of the occurrence of a strong MnO– TiO_2 interaction, as suggested in the literature [32].

3.2. STEM-EELS

Fig. 3 shows two chemical maps (images a and b (Fig. 6)) obtained for the Co/Mn/TiO_2 catalyst after calcination, with different colors denoting the three elements (Co = red, Ti = green, Mn = blue). Image a (Fig. 4) is composed of a large TiO_2 particle, which supports three small Co_3O_4 particles with sizes in the range of ~ 12 to 18 nm . It can easily be seen that the MnO_x species are located preferentially with the Co_3O_4 particles, leading to the purple (red + blue) particles in the image. It appears as if a mixed compound between Co and Mn is formed and/or that MnO_x species cover the surface of Co_3O_4 . Another example is shown in image b (Fig. 4), where a Co_3O_4 particle around ~ 14 – 17 nm in size is observed, and some very small Mn spots decorate the particle. The possible formation of a solid solution is considered since Co and Mn atoms have a similar ionic radius and can form stable mixed oxides. Thus, during the calcination Mn^{n+} cations are likely to replace either the octahedral or tetrahedral sites in the Co_3O_4 structure, leading to the formation of a mixed spinel compound of the type $\text{Mn}_x\text{Co}_{3-x}\text{O}_4$. The formation and composition of these Co/Mn mixed compounds have been the subject of numerous works [28,33],

Table 2
FTS catalytic performances of Co/TiO_2 and Co/Mn/TiO_2 at 220°C and 1, 4, 8, and 18 bars

Catalyst	Pressure (bar)	Co-time yield ^a	Selectivity (wt%)		α values ^b
			CH_4	C_{5+}	
Co/TiO_2	1	2.2	29	43	0.69
	4	2.1	28	56	0.81
	8	2.6	32	51	0.80
	18	2.5	32	55	0.79
Co/Mn/TiO_2	1	3.2	24	46	0.71
	4	2.8	22	64	0.84
	8	3.0	26	59	0.80
	18	4.0	27	59	0.83

^a Co-time yield: $10^{-6} \text{ mol}_{\text{CO}}/(\text{g}_{\text{Co}} \text{ s})$.

^b As calculated from the slope between C_3 and C_7 in the ASF distribution plot, according to the equation $\log W_n/n = \log(\ln^2 \alpha) + n \log \alpha$, where W_n is the weight fraction of the products with n carbon number.

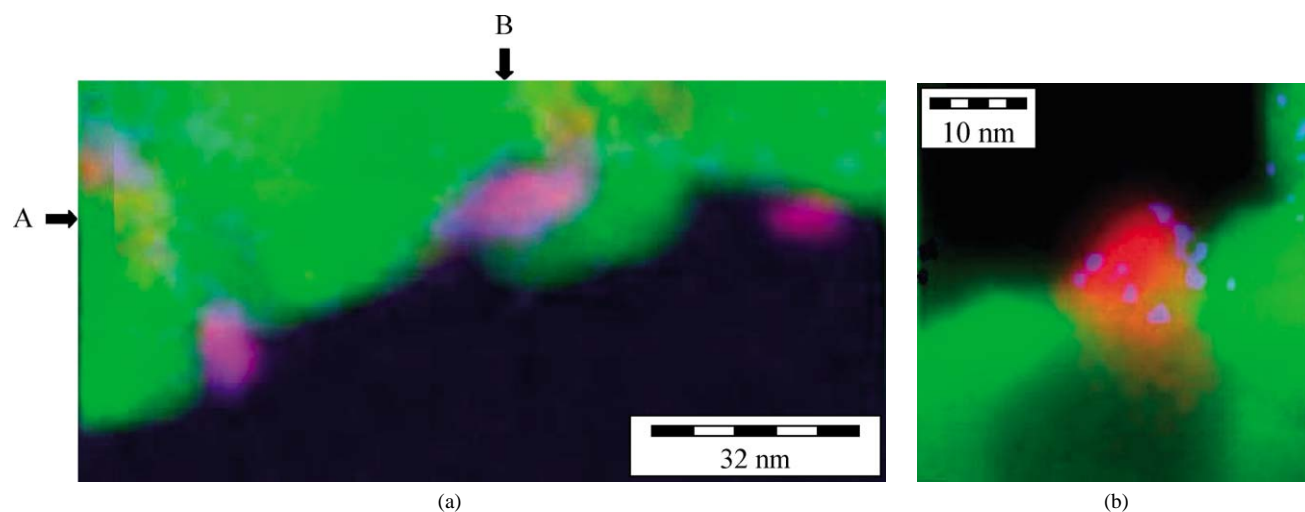


Fig. 4. STEM-EELS images: (a) $128 \times 64 \text{ nm}$, and (b) $40 \times 40 \text{ nm}$, of Co/Mn/TiO_2 catalyst after calcination (Co = red, Mn = blue, Ti = green). The arrows indicate the positions of the line scans that are given in Fig. 5.

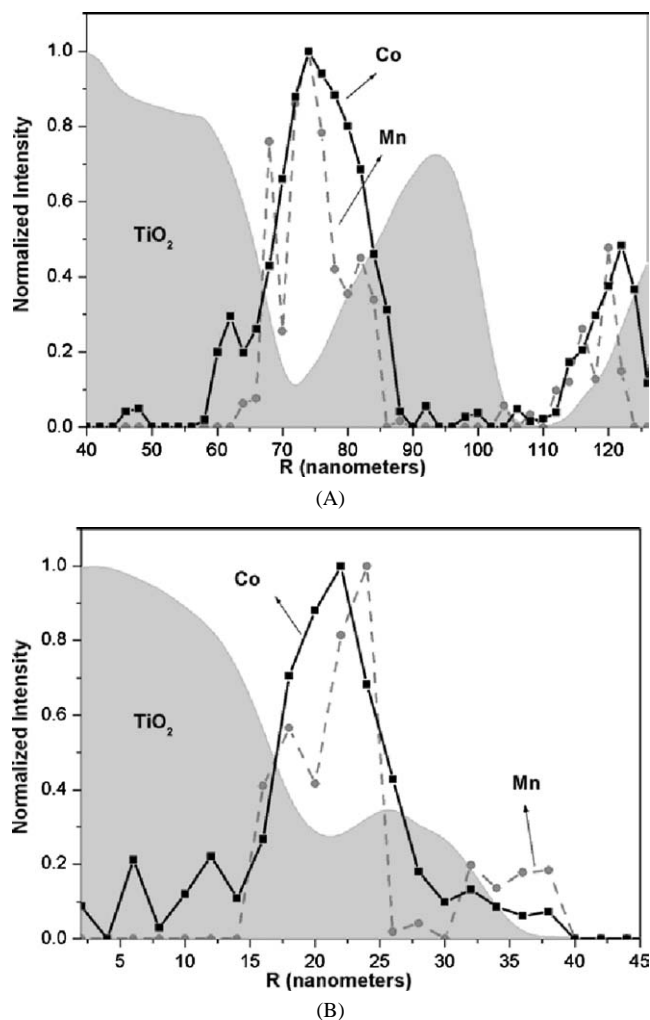


Fig. 5. Line scans carried out on the image a (Fig. 4). The scan A is a line that runs from the left to the right. The first 40 nm of TiO₂ has been omitted. Scan B is a vertical line starting from the top.

and their final composition is thought to depend on the Mn amount as well as on the temperature treatments carried out during their synthesis. With these results we do not rule out the presence of some amounts of MnO_x located over the TiO₂ surface, as can be seen on the right side of image b (Fig. 4). Nonetheless, it is clear that after calcination most of the Mn ions tend to coexist with the Co₃O₄, and a minor fraction is spread over the TiO₂ surface. A detailed investigation of the electronic state of the MnO_x compounds and their interaction with the support in TiO₂-supported catalysts will be addressed in a future publication.

In Fig. 5 two line scans performed on image a (Fig. 4) are presented (scans A and B). These line scans provide information about the relative intensity of each element along the scanned region. The intensities of Ti, Mn, and Co have all been normalized to 1. Because of the low Mn concentration, we considered a reliable quantitative determination of the concentration to be infeasible. In addition, the low concentration areas of Mn have been smoothed. The area below the TiO₂ curve is filled with grey to indicate the surface topog-

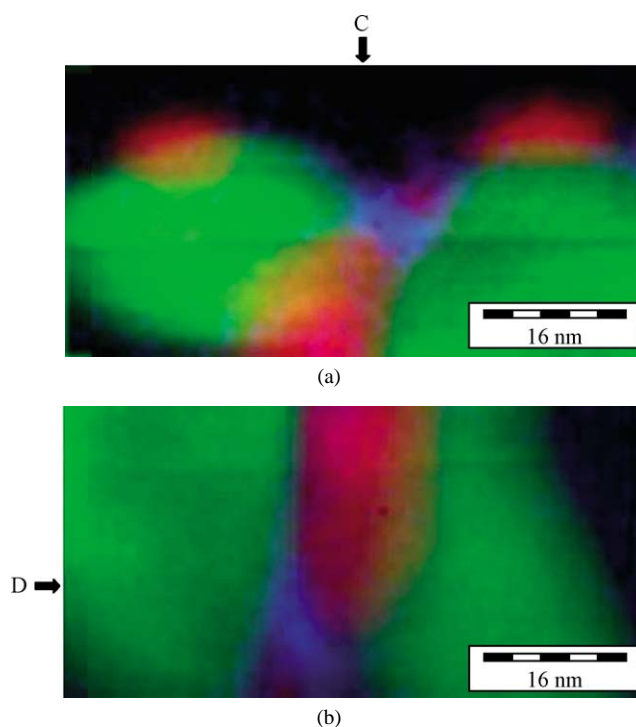


Fig. 6. STEM-EELS images (64 × 32 nm) of Co/Mn/TiO₂ catalyst after reduction at 350 °C in H₂ for 12 h and passivation at 150 °C in CO₂ (Co = red, Mn = blue, Ti = green). The arrows indicate the positions of the line scans that are given in Fig. 7.

raphy. Scan A runs from left to right in Fig. 4a, as indicated by the arrow, where the first 40 nm has been omitted from Fig. 4. It can be observed that the Co₃O₄ particles are located in the pores of the TiO₂ and that Mn and Co signals follow a similar intensity profile. Scan B runs from the top of the image (indicated by another arrow) into the vacuum. Scan B runs through the same Co/Mn (oxide) particle, and again it is observed that the amounts of Co and Mn are associated and fill a pore of the TiO₂ surface.

After reduction and passivation, a different situation is observed in terms of the Mn location. This is shown in Fig. 6, which contains two chemical maps (images a and b) of the reduced/passivated Co/Mn/TiO₂ catalyst. In image a, three Co⁰ particles are observed at the edges of the TiO₂ support. The size of these Co⁰ particles is in a range (14–18 nm) similar to that observed before reduction. However, as expected from the XPS data, Mn is no longer mixed with the Co⁰ particles. Instead, the MnO is dispersed over the TiO₂ support and is more concentrated close to the Co⁰ particles. In the second example (image b), a large Co⁰ particle is observed between two TiO₂ particles and the MnO is again located in the proximity of the Co⁰. We note that if the MnO is very highly dispersed, it is difficult to make it visible in the images because of the low signal/noise ratio, and therefore an evaluation of the EELS spectra is required to provide evidence of the existence of MnO. In images a and b (Fig. 6) we mainly captured the MnO clustering in the vicinity of the

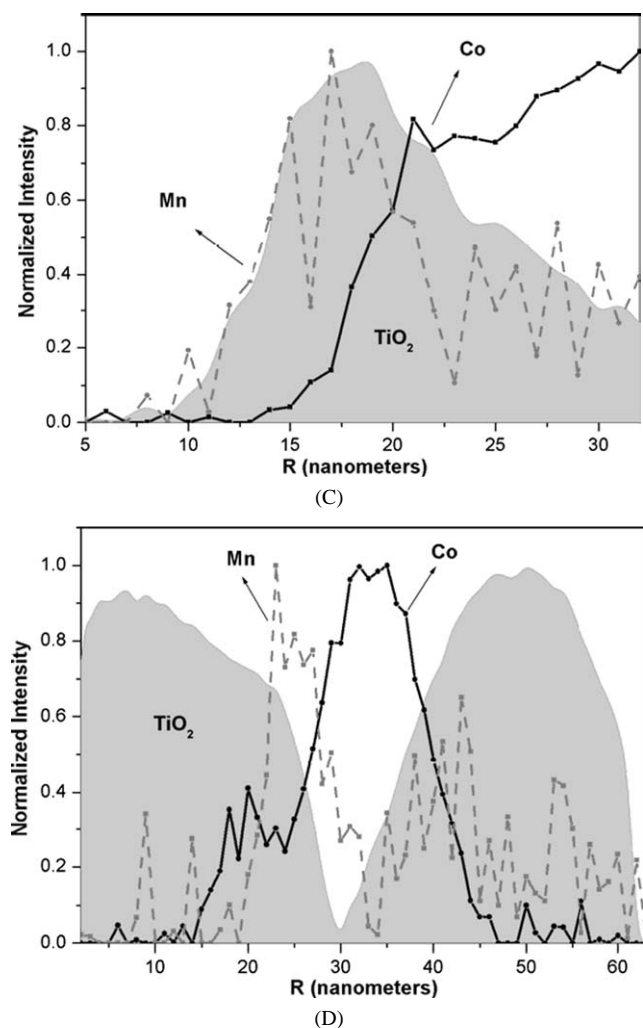


Fig. 7. Line scans carried out on images a and b (Fig. 6). Scan C is a line that runs from the left to the right. Scan D is a vertical line starting from the top.

Co particles, although the MnO was also detected in a very low concentration throughout the surface of the TiO₂.

In Fig. 7 two other line scans are presented (scans C and D), which were performed on images a and b (Fig. 6), respectively. Scan C runs from the top of image a (Fig. 6) to the bottom, as indicated by an arrow. The Mn signal is now associated more with the TiO₂, given that the intensity profiles follow a similar trend, whereas the Co signal follows an opposite trend, indicating that the Co⁰ particle remains located in a pore of the TiO₂ surface. However, a clear interface between the Co and Mn particles can be observed, confirming that a certain Co–Mn interaction remains after reduction. Moreover, a weak Mn signal is still observed along the Co⁰ particle, suggesting the presence of small MnO particles associated with the Co⁰. Scan D runs from the left side of image b (Fig. 6), starting from the arrow to the right. Again, a clear Co–Mn interface is observed, which is indicative of the proximity of the Co⁰ and MnO compounds.

With these STEM-EELS images we prove that the location of the Mn promoter is highly related to the surface composition of the catalyst and that the formation of mixed compounds between Co and Mn, under certain conditions, can be energetically favorable. With the above findings we establish, to the best of our knowledge, for the first time in this type of catalytic system, the spatial location of the Mn promoter, which will be of interest for the development of improved Co-based FTS catalysts in the near future.

3.3. Catalytic testing

The catalytic performances of Co/TiO₂ and Co/Mn/TiO₂ were compared after 22 h of FTS reaction at 1 bar and consecutively after 8 h at 4, 8, and 18 bar. We calculated the activities as the percentage CO converted into hydrocarbons without taking into account other side reactions (i.e., CO₂ formation). Table 2 summarizes the catalytic performances for both catalysts at different pressures. The Co/Mn/TiO₂ catalyst gives a higher Co-time yield than the Co/TiO₂ catalyst at all pressures. The activity increases slightly from 1 to 18 bar, from 2.2 to 2.5 × 10⁻⁶ mol_{CO}/(g_{Co} s) in Co/TiO₂ and from 3.2 to 4.0 × 10⁻⁶ mol_{CO}/(g_{Co} s) in Co/Mn/TiO₂. These higher Co-time yields obtained with Co/Mn/TiO₂ are not caused by a higher Co dispersion, since H₂ chemisorption measurements gave similar values for the two catalysts. Hence, the increase in activity is induced by the presence of MnO as a promoter. Furthermore, the MnO leads to an enhancement of the selectivity in the Co/Mn/TiO₂ catalyst, in which the weight percentage of C₅₊ is always higher than it is in the Co/TiO₂ catalyst. This is mainly caused at the expense of CH₄ production, which decreases by 4 to 7 wt% in Co/Mn/TiO₂ at all pressures. Moreover, a slight increase in the chain growth probability (α) is obtained because of the effect of MnO, from 0.69 to 0.71 at 1 bar and from 0.79 to 0.83 at 18 bar. These results indicate a different favorable termination path of the growing alkyl chain during FTS as a result of the presence of MnO in the catalyst. We attribute this suppression of CH₄ formation to a decrease of the hydrogenation rate, which favors the formation of higher hydrocarbons (C₅₊). This might be related to a lower capacity of the Mn-promoted catalyst to chemisorb hydrogen, which is affected by the higher amount of Co^{δ+} in the active catalyst [18]. It has been proposed that MnO can play a role as a co-catalyst, providing new active sites for the formation and stabilization of C_xH_yO_z intermediates [34]. These intermediates would be formed by CO insertion into a CH_x group adsorbed on a Co⁰ site, provided that MnO is located at the interphase of the Co⁰ particles. In the present work we have shown that MnO particles are located in the vicinity of the Co⁰ particles, and thus they may form new sites that are active for the insertion of CO into the growing alkyl chains, which would be subsequently hydrogenated on the metallic Co⁰ surface. This MnO is inactive in the absence of Co⁰, since the latter is needed to dissociate the

H₂ and hydrogenate the intermediate compounds. This argument would explain the higher activities obtained with the Mn-promoted catalysts and the decrease in the hydrogenation rate, which leads to CH₄ suppression. Further investigations are needed to elucidate how the MnO modifies the reaction mechanism and, hence, the selectivity of FTS catalysts.

4. Conclusions

The addition of Mn to a Co/TiO₂-based Fischer–Tropsch catalyst causes a decrease in the reducibility of Co₃O₄ and results in a less metallic behavior by the active catalyst. The presence of Mn leads to the possible formation of a solid solution in the calcined catalyst, wherein Mnⁿ⁺ cations are incorporated into the Co₃O₄ structure, resulting in the formation of a mixed oxidic phase Mn_xCo_{3-x}O₄. On the other hand, H₂ reduction gives rise to a partially reduced Co⁰ phase and the migration of the MnO particles toward the TiO₂. However, a certain Co–Mn interaction remains, since MnO clusters are frequently observed in the vicinity of the Co⁰ particles. We assume that the presence of these MnO compounds near the Co⁰ affects the electronic properties of these sites, as previously measured by soft X-ray absorption spectroscopy, and therefore induces changes in the surface coverage and reaction pathways during FTS. The MnO might also play a role as a co-catalyst by providing extra sites where CO insertion into the growing alkyl chains happens. This can only occur when MnO particles are located close to the interphase with the metallic Co⁰. Hence, the Co–Mn interaction gives rise to the observed promotion effect in FTS. This promotion effect becomes apparent as a suppression of CH₄ formation, an increase in the C₅₊ selectivity, and an enhancement of the Co-time yield.

Acknowledgment

The authors gratefully acknowledge financial support from Shell Global Solutions and the University de Nord (Paris) for TEM-EELS measurements. The authors acknowledge H. Oosterbeek and H.P. Calis for the high-pressure catalytic tests. The work also benefited from fruitful discussions with H. Oosterbeek, H.P.C. Kuipers, and C. Mesters of Shell Global Solutions.

References

- [1] J.J. Mortensen, B. Hammer, J. Norskov, Phys. Rev. Lett. 80 (1998) 4333.
- [2] J.G. Serafin, A.C. Liu, S.R. Seyedmonir, J. Mol. Catal. 131 (1998) 157.
- [3] R.A. van Santen, H.P.C. Kuipers, Adv. Catal. 35 (1987) 265.
- [4] J.R. Rostrup-Nielsen, Catal. Today 71 (2002) 243.
- [5] E. Iglesia, Appl. Catal. A: Gen. 161 (1997) 59.
- [6] C.H. Bartholomew, R.C. Reuel, Ind. Eng. Chem. 24 (1985) 56.
- [7] G.L. Bezemer, A. van Laak, A.J. van Dillen, K.P. de Jong, Stud. Surf. Sci. Catal. 147 (2004) 259.
- [8] S. Vada, A. Hoff, E. Adnanes, D. Schanke, A. Holmen, Top. Catal. 2 (1995) 155.
- [9] G. Jacobs, M. Patterson, Y. Zhang, T. Das, J. Li, B.H. Davis, Appl. Catal. A: Gen. 233 (2002) 215.
- [10] E. Iglesia, S.L. Soled, R.A. Fiato, G.H. Via, J. Catal. 143 (1993) 345.
- [11] J. Barrault, Stud. Surf. Sci. Catal. 11 (1982) 225.
- [12] M. van der Riet, R.G. Copperthwaite, G.J. Hutchings, J. Chem. Soc. Faraday Trans. 83 (1987) 2963.
- [13] T. Riedel, M. Cleys, G. Schulz, G. Schaub, S. Nam, K. Jun, M. Choi, G. Kishan, K. Lee, Appl. Catal. A: Gen. 186 (1999) 201.
- [14] M.J. Keyser, R.C. Everson, R.L. Espinoza, Appl. Catal. A: Gen. 171 (1998) 99.
- [15] H. Kölbl, F. Engelhard, Erdöl und Kohle 2 (1949) 52.
- [16] F. Morales, O.L.J. Gijzeman, F.M.F. de Groot, B.M. Weckhuysen, Stud. Surf. Sci. Catal. 147 (2004) 271.
- [17] O. Stephan, A. Gloter, D. Imhoff, M. Kociak, K. Suenaga, M. Tence, C. Colliex, Surf. Rev. Lett. 7 (2000) 475.
- [18] F. Morales, F.M.F. de Groot, P. Glatzel, E. Kleimenov, H. Bluhm, M. Havecker, A. Knop-Gericke, B.M. Weckhuysen, J. Phys. Chem. B 108 (2004) 16201.
- [19] D.A. Shirley, Phys. Rev. B 5 (1972) 4709.
- [20] J.H. Scofield, J. Electron Spectrosc. Relat. Phenom. 8 (1976) 129.
- [21] R. Riva, H. Miessner, R. Vitali, G. Del Piero, Appl. Catal. A: Gen. 196 (1999) 111.
- [22] K.J. Kim, Y.R. Park, Solid State Commun. 127 (2003) 25.
- [23] K. Okada, A. Kotani, J. Phys. Soc. Jpn. 61 (1992) 449.
- [24] J. van Elp, J.L. Wieland, H. Eskes, P. Kuiper, G.A. Sawatzky, F.M.F. de Groot, T.S. Turner, Phys. Rev. B 44 (1991) 6090.
- [25] Y. Brik, M. Kacimi, M. Ziyad, F. Bonzon-Verduraz, J. Catal. 202 (2001) 118.
- [26] J.L. Gautier, E. Rios, M. Gracia, J.F. Marco, J.R. Gancedo, Thin Sol. Films 311 (1997) 51.
- [27] D. Briggs, M.P. Seah (Eds.), Practical Surface Analysis, vol. 1, second ed., Wiley, New York, 1994, p. 128.
- [28] Q. Liang, K. Chen, W. Hou, Q. Yan, Appl. Catal. A: Gen. 166 (1998) 191.
- [29] L.A. Boot, M.H.J.V. Kerkhoffs, B.T. van der Linden, A.J.V. Dillen, J.W. Geus, F.R. van Buren, Appl. Catal. A 137 (1996) 69.
- [30] K. Hadjiivanov, D. Klissurski, A. Davydov, J. Chem. Soc. Faraday Trans. 1 84 (1998) 34.
- [31] K. Hadjiivanov, J. Lamotte, J. Lavalley, Langmuir 13 (1997) 3374.
- [32] M. Kantcheva, M.U. Kucukkal, S. Suzer, J. Catal. 190 (2000) 144.
- [33] J.L. Martin de Vidales, E. Vila, R. Rojas, O. Garcia, Chem. Mater. 7 (1995) 1716.
- [34] H. Treviño, T. Hyeon, W.M.H. Sachtler, J. Catal. 170 (1997) 236.